Design of orthogonally jointed 2D transition metal dichalcogenide heterojunctions for enhanced Photoelectrochemical water reduction

Chih-hung Wu,[a] Keng-Hung Chang,[a] Yu-Hao Tu,[b] Chen-Hao Yeh,[c] Heng-Jui Liu*[a]

[a] *Department of Materials Science and Engineering, National Chung Hsing University, Taichung 402202, Taiwan*

[b] *College of Semiconductor Research, National Tsing Hua University, Hsinchu 300044, Taiwan*

[c] Department of Materials Science and Engineering, Feng Chia University, Taichung 407012, Taiwan

Corresponding Author

*e-mail: hengjui0109@dragon.nchu.edu.tw

Table S1 Surface elemental compositions for all samples from XPS survey scan

Sample	Mo (at%)	W (at%)	S (at%)	O (at%)
MoS_2/p-Si	37.6	—	52.7	9.7
WS_2/p-Si	—	34.0	41.8	24.2
orth-MoS_2/WS_2/p-Si	36.9	3.9	49.2	10.1
orth-WS_2/MoS_2/p-Si	3.6	36.2	44.1	16.1

Table S2 Fitting result of Nyquist plots for all samples

Sample	Rs (Ω)	R_{ct1} (Ω)	R_{ct2} (Ω)
MoS_2/p-Si	190	2634	—
WS_2/p-Si	265.8	1937	—
orth-MoS_2/WS_2/p-Si	124.2	263.3	745.9
orth-WS_2/MoS_2/p-Si	134.8	348.6	473.3

Table S3 Calculated adsorption energy (in eV) of a hydrogen atom on all potential active sites of three different WS_2/MoS_2 heterostructures.

Vertically joined WS_2/MoS_2		Laterally stacking WS_2/MoS_2		Horizontally joined WS_2/MoS_2	
Site	E_{ads} (eV)	Site	E_{ads} (eV)	Site	E_{ads} (eV)
H1	-4.32	**H1**	-1.52	**H1**	-1.52
H2	-2.47	**H2**	-1.50	**H2**	-1.52
H3	-2.73	**T1**	-1.28	**H3**	-1.58
H4	-2.89			**T1**	-1.54
H5	-3.29			**T2**	-1.50
H6	-3.29			**T3**	-1.75
T1	-4.32				
T2	-2.73				
T3	-3.17				
T4	-2.32				
T5	-2.45				

Table S4 Convergence tests for various Monkhorst-Pack k-points for the adsorption energy of hydrogen atom on the most stable adsorption site on the WS_2/MoS_2 heterostructure.

	Vertically joined WS_2/MoS_2	Laterally stacking WS_2/MoS_2	Horizontally joined WS_2/MoS_2
grid	E_{ads} (eV)	E_{ads} (eV)	E_{ads} (eV)
3 × 3 × 1	-4.321	-1.520	-1.755
4 × 4 × 1	-4.322	-1.521	-1.754
5 × 5 × 1	-4.322	-1.521	-1.754
6 × 6 × 1	-4.322	-1.520	-1.754
7 × 7 × 1	-4.322	-1.521	-1.754

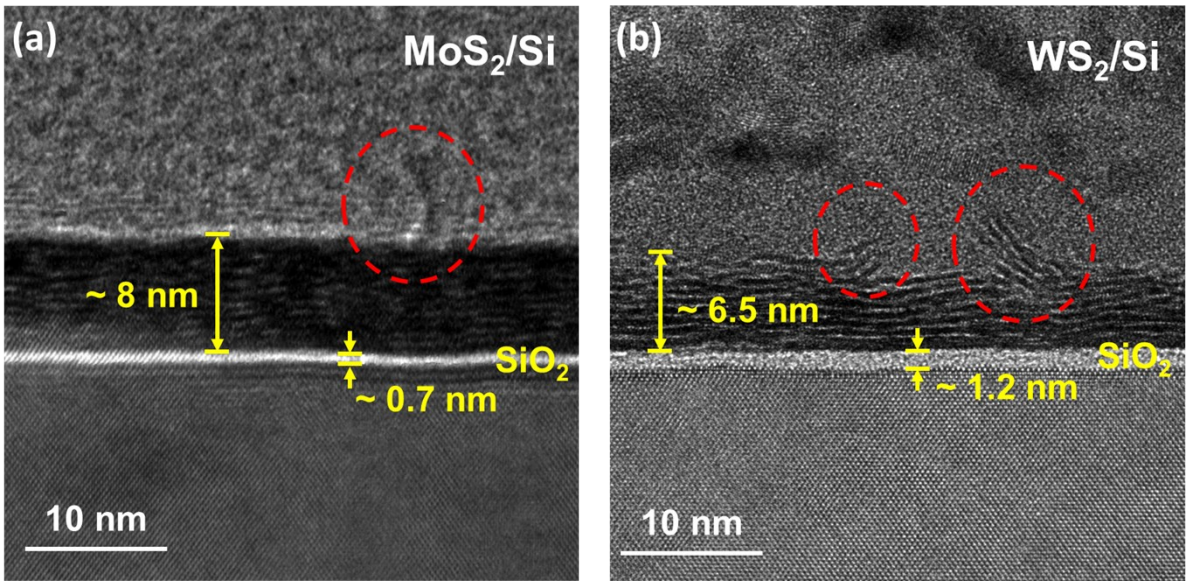

Fig. S1 Cross-sectional HR-TEM images of single-component (a) MoS_2/p-Si and (b) WS_2/p-Si heterostructures. The images reveal that MoS_2 and WS_2 initially follow a layer-by-layer growth mode, maintaining a horizontally stacking structure below a critical thickness of ~8 nm and ~6.5 nm, respectively. However, as the growth approaches these critical thicknesses, slight vertical protrusions also emerge, serving as seeds for the subsequent formation of vertically standing TMD nanosheets. Note that an ultrathin SiO_2 layer of below 1.2 nm is inevitably formed during the growth process of these TMD layers.

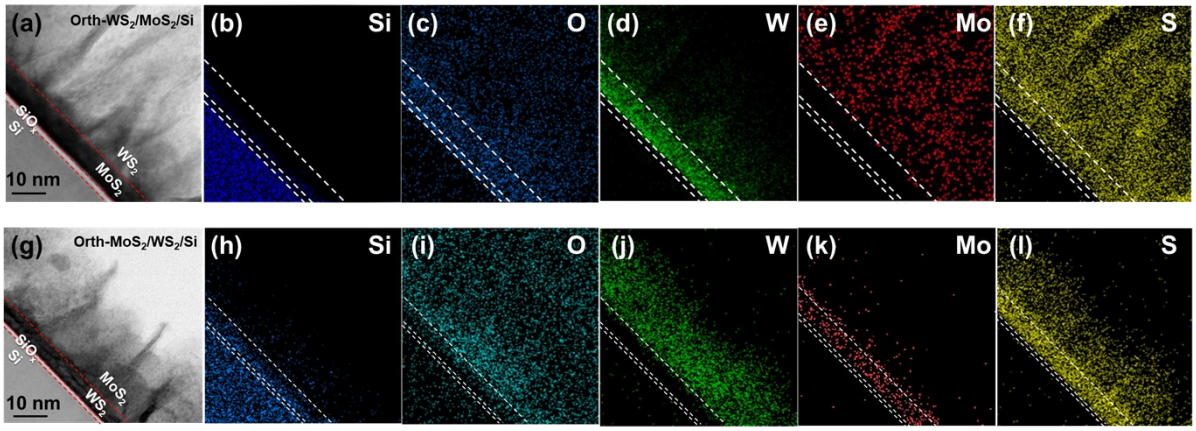

Fig. S2. (a–f) Cross-sectional bright-field (BF) HR-TEM image and corresponding EDS elemental maps of Si, O, W, Mo, and S for the orth-WS_2/MoS_2/Si heterostructure. (g–l) Cross-sectional BF HR-TEM image and EDS elemental maps of Si, O, W, Mo, and S for the orth-MoS_2/WS_2/Si heterostructure. The red and white dashed lines are aligned at identical relative positions across each panel to guide the eye in identifying the layer constituents. An ultrathin SiO_x interlayer can be observed between the first TMD layer and the Si substrate, appearing as the brightest contrast in the BF images, with overlapping Si and O signals confirmed in the corresponding EDS maps.

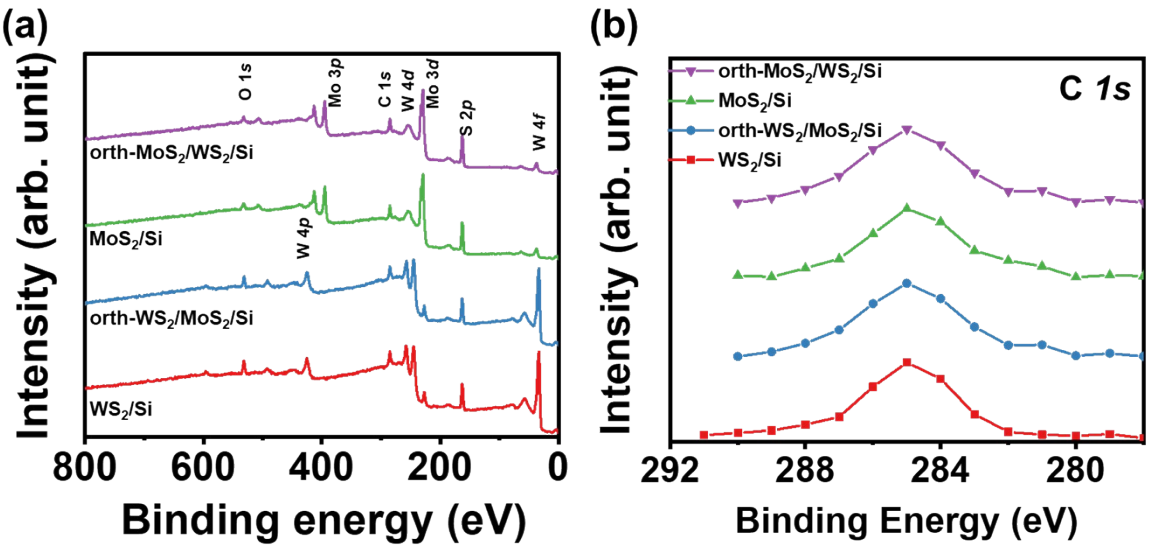

Fig. S3. (a) the survey scans and (b) the C 1s spectra for all samples. In the C 1 spectra, all curves show a characteristic peak at 284.8 eV from adventitious carbon, indicating similar levels of surface contamination across all samples.

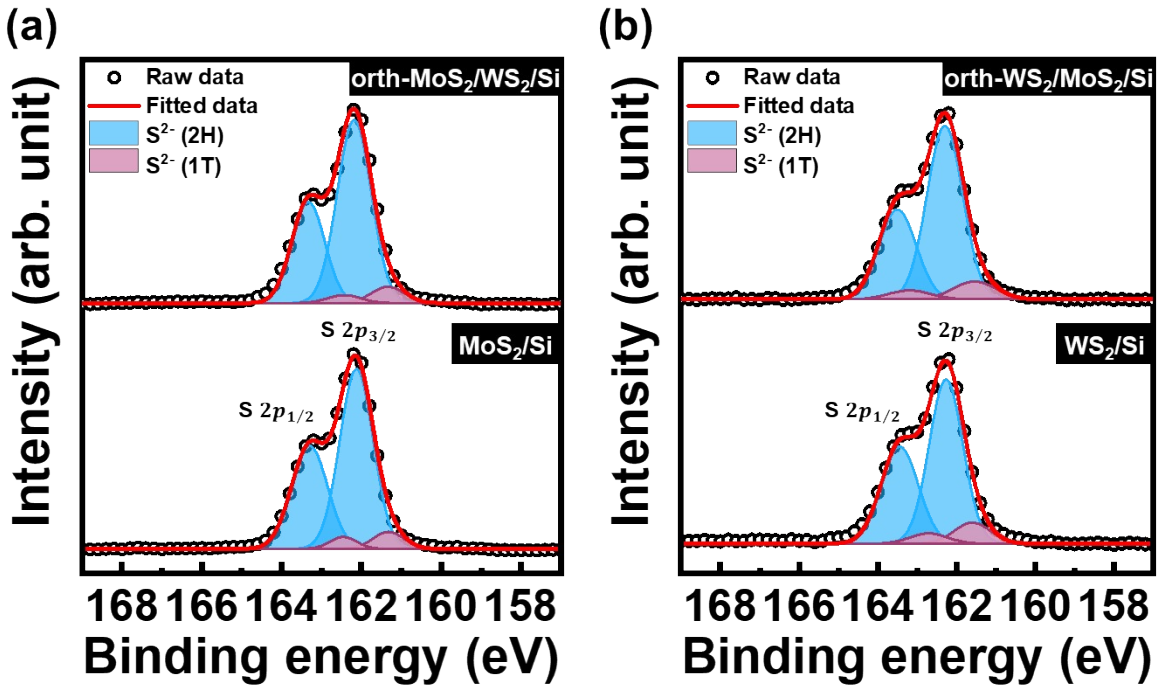

Fig. S4. (a) S 2*p* XPS spectra for the orth-MoS_2/WS_2/p-Si heterostructure and single-component MoS_2/p-Si heterostructure. (b) S 2*p* XPS spectra for the orth-WS_2/MoS_2/p-Si heterostructure and single-component WS_2/p-Si heterostructure.

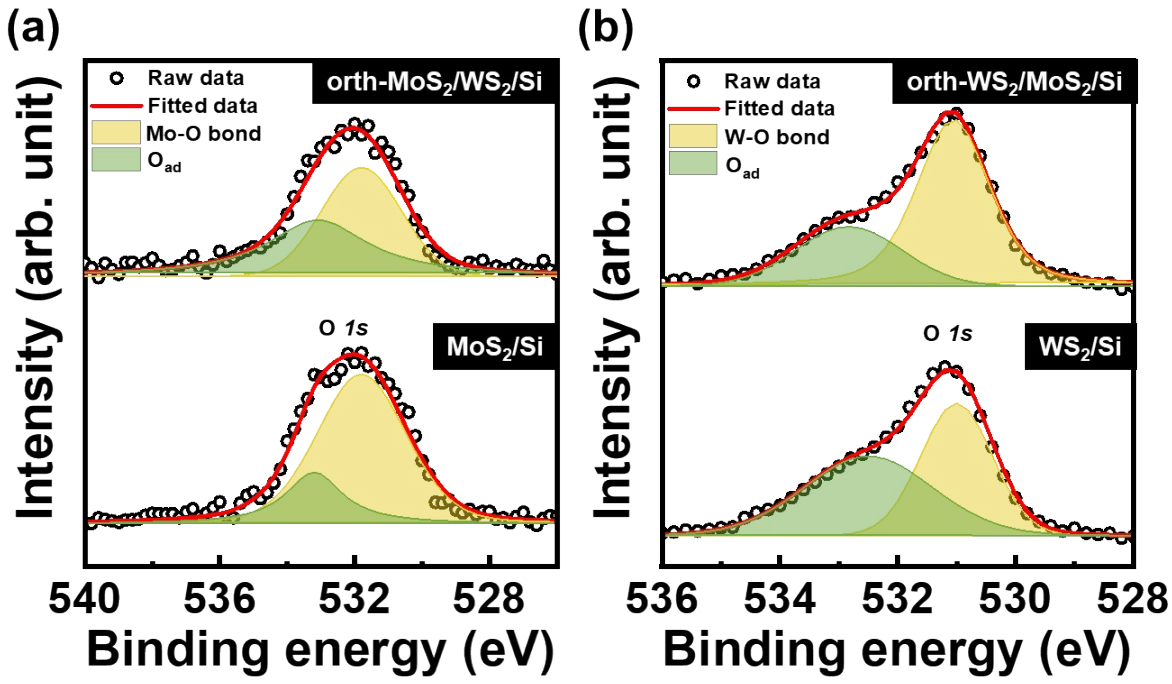

Fig. S5. (a) O 1*s* XPS spectra for the orth-MoS_2/WS_2/p-Si heterostructure and single-component MoS_2/p-Si heterostructure. (b) O 1*s* XPS spectra for the orth-WS_2/MoS_2/p-Si heterostructure and single-component WS_2/p-Si heterostructure.

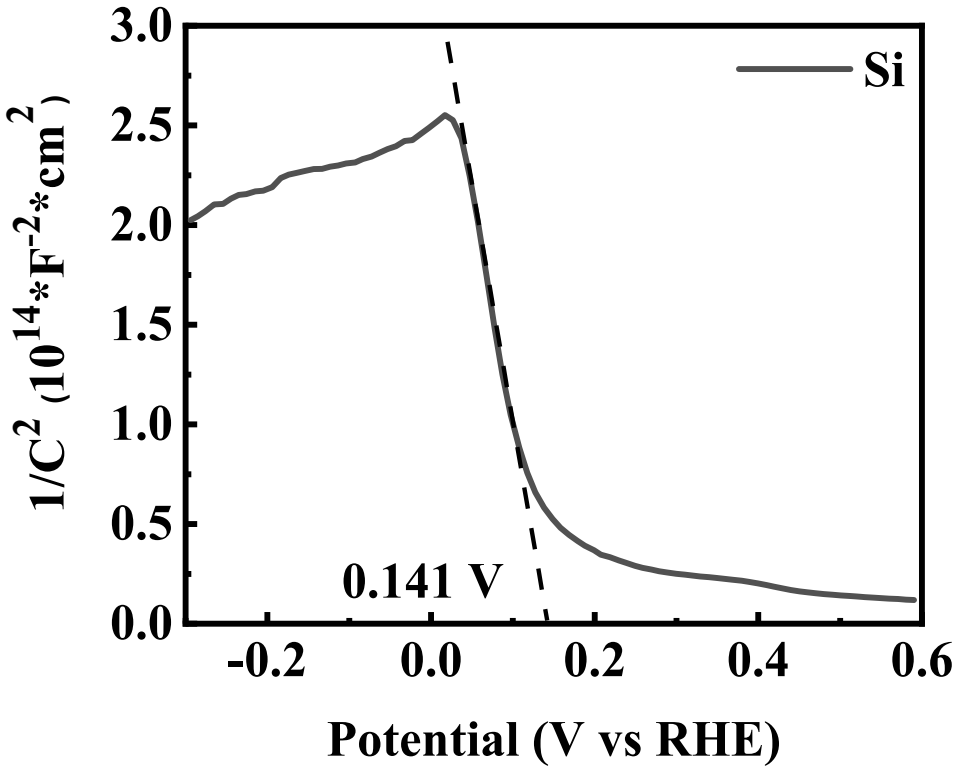

Fig. S6 Mott-Schottky plot of blank p-Si substrate.

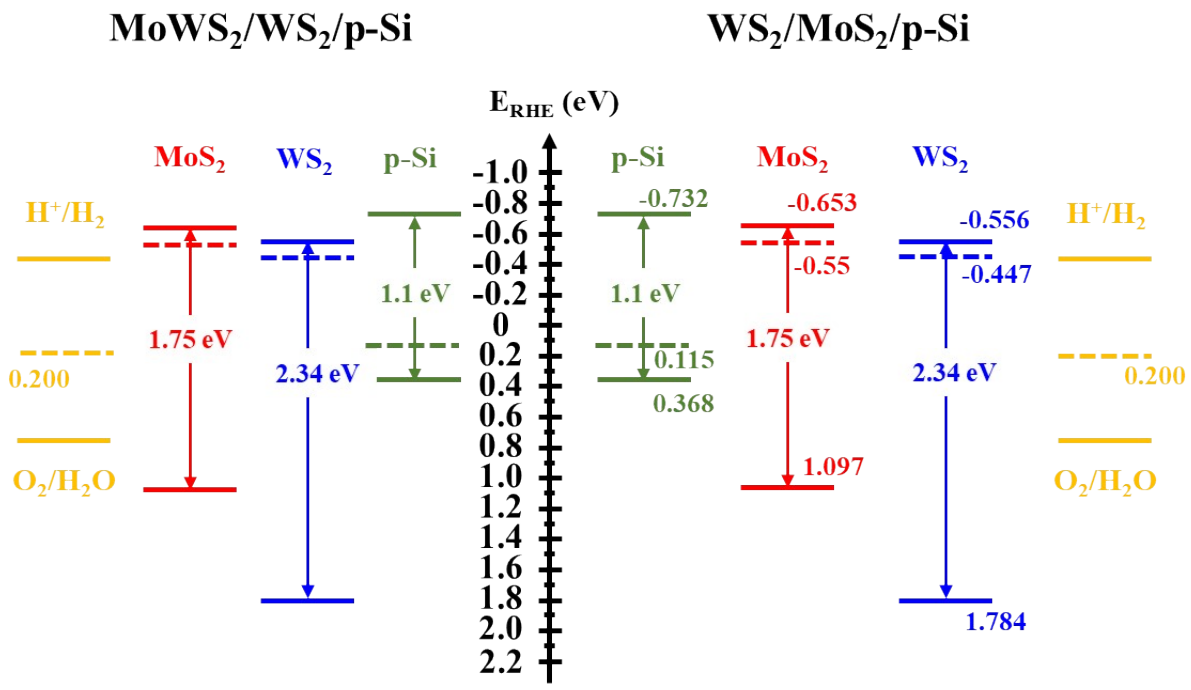

Fig. S7 Band alignment diagrams relative to E_{RHE} of orth-WS_2/MoS_2/p-Si (right) and orth-MoS_2/WS_2/p-Si (left) heterostructures are constructed according to the analysis of the Mott-Schottky plots of the single-component WS_2/p-Si and MoS_2/p-Si heterostructures. The details are unveiled below:

Analysis of Mott-Schottky measurement

1. The flat-band potential (V_{fb}) of the single-component WS_2/p-Si and MoS_2/p-Si heterostructures electrode is determined using the Mott-Schottky equation: [1]

$$C^{-2} = \frac{2\left(V - V_{fb} - {kT}/{e}\right)}{e\varepsilon_0\varepsilon_r N_D A^2}$$

Here, C is the space charge layer capacitance from Mott-Schottky measurements, e is the the elementary charge (~ 1.658×10^{-24} F), $\varepsilon_0$is the vacuum permittivity (~ 8.85×10^{-14} F/cm), ε_r is the relative permittivity (5.5 for MoS_2 and 5.9 for WS_2), V is the applied voltage, k is Boltzmann's constant (~8.62×10^{-5}eV/K), N_D is the carrier density, T is room temperature (300 K), and A is the electrode-electrolyte contact area.

The flat-band potential is obtained from the x-intercept (V_0) of the linear region of the Mott-Schottky plot using:

$$V_0 = V_{fb} + {kT}/{e}$$

From this, V_{fb} values are -0.55 and -0.47 V vs. RHE for MoS_2 and WS_2, respectively (with V_0 at -0.524 V and -0.421 V).

2. The donor carrier concentration (N_D) is derived from the slope of the Mott-Schottky plot (

$^2/e\varepsilon_0\varepsilon_r N_D A^2$), yielding $\sim 5.654 \times 10^{13} cm^4/F^2$ for WS_2/p-Si and $\sim 1.267 \times 10^{13} cm^4/F^2$ for MoS_2/p-Si, corresponding to N_D values of $4.085 \times 10^{22} cm^{-3}$ and $1.956 \times 10^{23} cm^{-3}$, respectively.

3. The conduction band edge (E_{CB}) is calculated as:

$$E_{CB} = V_{fb} + kTln(^{N_D}/_{N_{CB}})$$

Where N_{CB} is the effective conduction band density of states:

$$N_{CB} = 2\sqrt{(\frac{2\pi m_e^* kT}{h^2})^3}$$

where m_e^* as effective mass ($0.33m_0$ for WS_2 and $0.39m_0$ for MoS_2) and h is Planck's constant ($6.626 \times 10^{-34} J \cdot s$). This gives N_{CB} values of $4.746 \times 10^{24}\ cm^{-3}$ for WS_2 and $1.049 \times 10^{25}\ cm^{-3}$ for MoS_2. Therefore, the conduction band edges are -0.653 V for WS_2 and -0.556 V for MoS_2 vs. RHE.

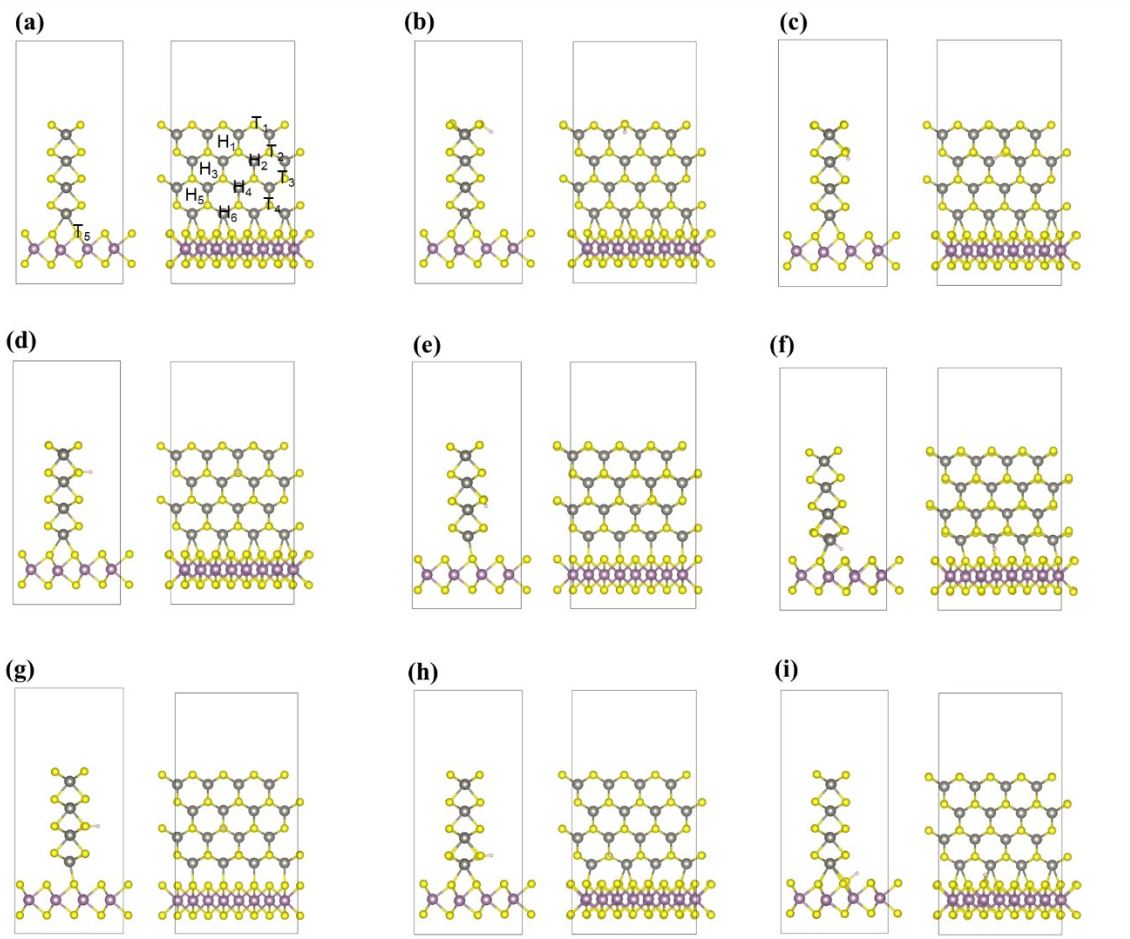

Fig. S8 (a) the possible adsorption sites in the orthogonally joined WS_2/MoS_2 heterostructure for the adsorbate, where the T and H represent the top and hollow sites; Optimized adsorption structures of a H atom on (b) H1 (= T1), (c) H2, (d) H3 (=T2), (e) H4, (f) H5 (=H6), (g) T3, (h) T4, and (i) T5 sites.

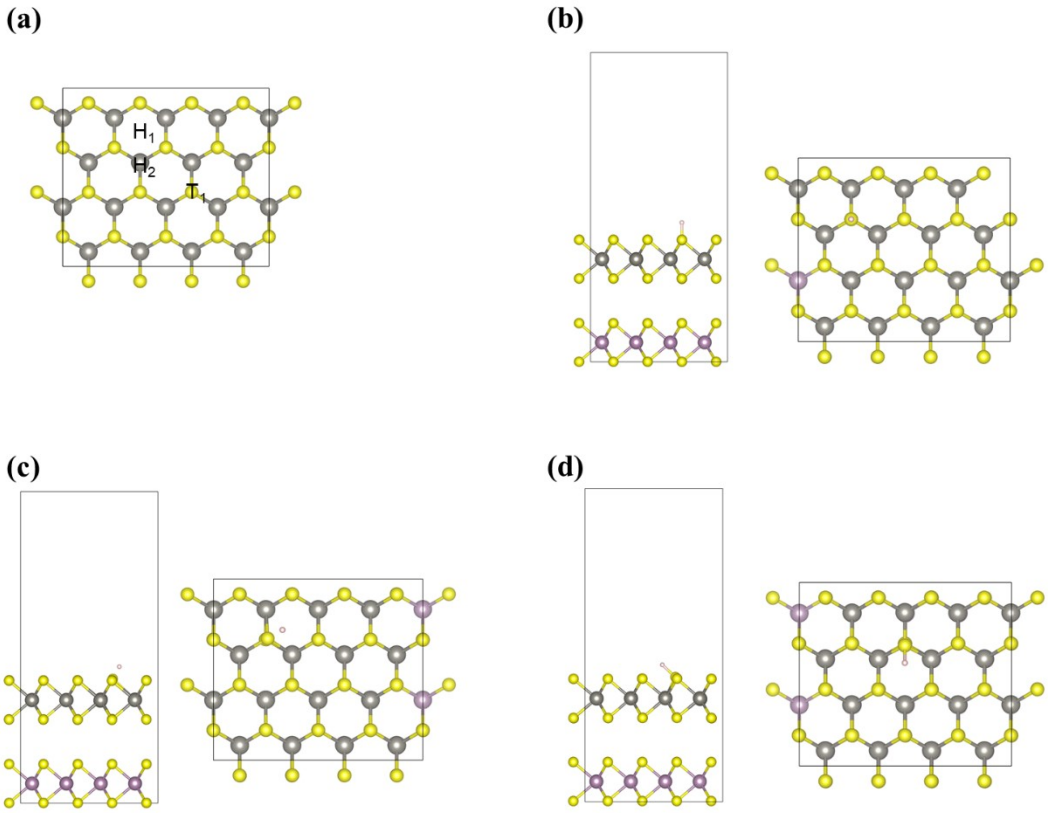

Fig. S9 (a) the possible adsorption sites in the vertically stacked WS_2/MoS_2 heterostructure for the adsorbate, where the T and H represent the top and hollow sites; Optimized adsorption structures of a H atom on (b) T1, (c) H1, and (d) H2 sites. We only considered the WS_2 side since the MoS_2 side is connected to the p-Si.

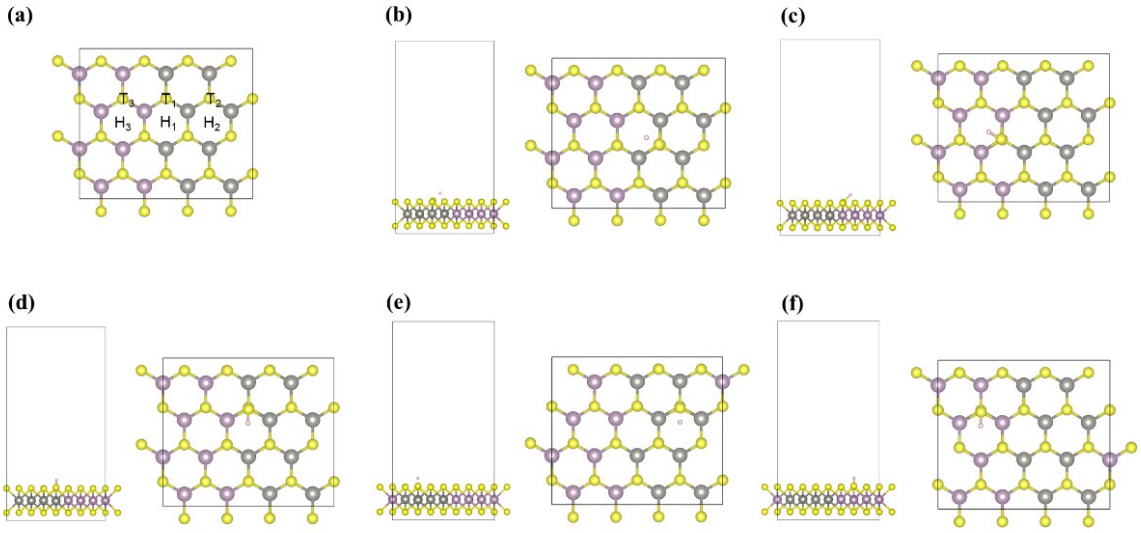

Fig. S10 (a) the possible adsorption sites in the in-plane interconnected WS_2/MoS_2 heterostructure for the adsorbate, where the T and H represent the top and hollow sites; Optimized adsorption structures of a H atom on (b) H1 (=H2), (c) H3, (d) T1, (e) T2, and (f) T3 sites.

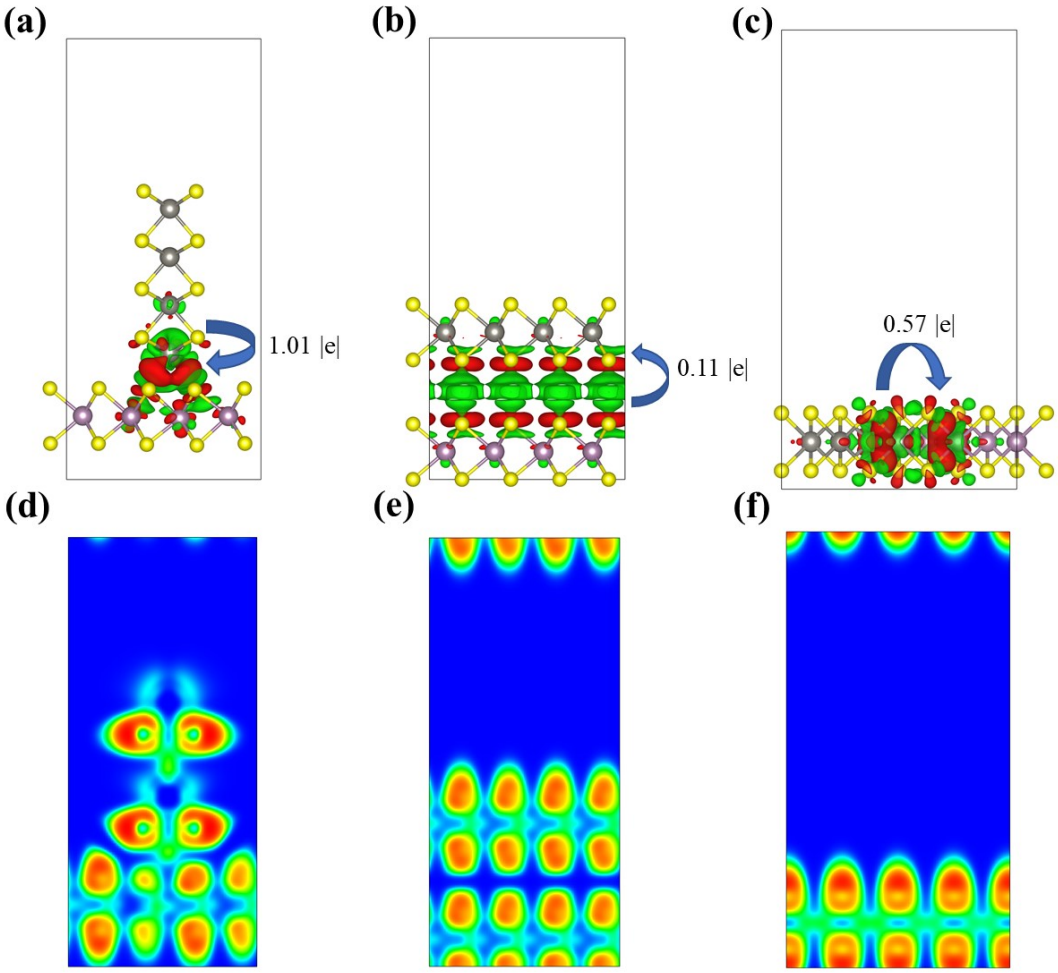

Fig. S11 Calculated charge density difference (CDD) diagrams of (a) orthogonally jointed (isosurface level: 0.05 |e|/Bohr^3), (b) vertically stacked (isosurface level: 0.00005 |e|/Bohr^3), and (c) in-plane interconnected WS_2/MoS_2 (isosurface level: 0.005 |e|/Bohr^3) heterostructures. The Green and red represent the region of electron depletion and accumulation, respectively. Calculated electron localization function (ELF) diagrams of (d) orthogonally jointed, (e) vertically stacked, and (f) in-plane interconnected WS_2/MoS_2 heterostructures.

Reference:

(1) Li, F.-S.; Fang, Y.-W.; Wu, Y.-T.; Wu, S.-W.; Ho, S.-Z.; Chen, C.-Y.; Chiang, C.-Y.; Chen, Y.-C.; Liu, H.-J. Self-Enhancement of Water Electrolysis by Electrolyte-Poled Ferroelectric Catalyst. *ACS Nano* **2023**, *17* (16), 16274-16286. DOI: 10.1021/acsnano.3c06371.